https://doi.org/10.1016/j.buildenv.2021.108027

Zhou, Y., An, Y., Chen, C., and You, R.* 2021. Exploring the feasibility of predicting contaminant transport using a stand-alone Markov chain solver based on measured airflow in enclosed environments. ***Building and Environment***, 202: 108027.

Exploring the Feasibility of Predicting Contaminant Transport Using a Stand-Alone Markov Chain Solver Based on Measured Airflow in Enclosed Environments

Yiding Zhou[1], Yuting An[1], Chun Chen[1,2], Ruoyu You[3,*]

[1] Department of Mechanical and Automation Engineering, The Chinese University of Hong Kong, Shatin, N.T. 999077, Hong Kong SAR, China

[2] Shenzhen Research Institute, The Chinese University of Hong Kong, Shenzhen 518057, China

[3] Department of Building Services Engineering, The Hong Kong Polytechnic University, Kowloon 999077, Hong Kong SAR, China

[*] Email: ruoyu.you@polyu.edu.hk

Abstract:

Correctly predicting contaminant transport in enclosed environments is crucial for improving interior layouts to reduce infection risks. Using the measured airflow field as input to predict the contaminant transport may overcome the challenges of measuring complex boundary conditions and inaccurate turbulence modeling in the existing methods. Therefore, this study numerically explored the feasibility of predicting contaminant transport from the measured airflow field. A stand-alone Markov chain solver was developed so that the calculations need not rely on commercial software. Airflow information from CFD simulation results, including the three-dimensional velocity components and turbulence kinetic energy, was used as surrogate for experimental measurement based on the spatial resolution of ultrasonic anemometers. Three cases were used to assess the feasibility of the proposed method, and the calculation results were compared with the benchmark calculated by the commercial CFD software. The results show that, when the airflow was simple, such as that in an isothermal ventilated chamber, the stand-alone Markov chain solver based on the measured airflow field predicted the trend of contaminant transport and peak concentrations reasonably well. However, for complex airflow, such as that in non-isothermal chambers with heat sources or occupants, the solver can reasonably predict only the general trend of contaminant transport.

Keywords:

Markov chain model; Airflow measurement; Contaminant; Computational fluid dynamics (CFD); Enclosed environment.

1. Introduction

In recent decades, transmission of airborne infectious diseases has become a major public concern. For example, outbreaks of measles [1], severe acute respiratory syndrome (SARS) [2], influenzas [3], and coronavirus disease 2019 (COVID-19) [4] have severely threatened human life and health. All these pandemics have been found to be related to the airflow patterns in enclosed environments [5], [6], [7]. If an infected person shares a living space with other occupants, the virus-containing droplets generated through talking, breathing, coughing, and sneezing can be transported by the airflow and inhaled by other occupants, resulting in cross-infection [8], [9]. In modern society, staying indoors at close proximity to other people is very common in daily life [10], and increases the chance of airborne diseases transmission. Therefore, correctly predicting contaminant transport in enclosed environments is important for improving interior layouts to reduce the risk of infection.

To predict contaminant transport in an existing indoor environment, a popular approach is to first conduct on-site measurements of the boundary conditions, then employ computational fluid dynamics (CFD) to calculate the airflow distribution, and finally use a contaminant transport model to make the prediction. For example, Zhang and Chen [11] first measured the boundary conditions, such as the supply air velocity, temperature and the rate of heat generation by occupants and equipment, in a ventilated room, and then used the renormalized group (RNG) k-ε model for airflow simulation and the Eulerian model to calculate the particle transport. Pan et al. [12] first measured boundary conditions such as supply air velocity in a laboratory chamber, and then used large eddy simulation (LES) to calculate the airflow and the Lagrangian model to predict the particle transport and deposition. Zhang et al. [13] first measured the air velocity from supply air diffusers and the temperatures in the boundary areas in an aircraft cabin mockup, and then calculated the airflow field using the RNG k–ε model and the particle dispersion with the Lagrangian model. These studies have provided great insight into approaches for predicting contaminant transport in existing indoor environments.

However, the accuracy of the methods above depends strongly on accurate calculation of the airflow distribution, which is challenging in practical applications. One challenge is the measurement of boundary conditions in some cases. For example, Zhang et al. [13] observed that it was not feasible to obtain detailed measurements of the three-dimensional air velocity distribution at inlets with the use of ultrasonic anemometers due to their large size. Chen et al. [14] ascribed significant discrepancies between simulation results and experimental data to inaccurate measurement of boundary conditions. Vidal et al. [15] found it difficult to determine and quantify boundary conditions in practice as it was extremely time consuming to measure all variables such as temperature, air velocity, and pressure drop. In addition, the existing turbulence models are not always accurate, especially for prediction of three-dimensional air velocity components and turbulence quantities. For example, although the RNG k-ε model was found to have the best overall performance in calculating the airflow distribution in indoor environments [16], Wang and Chen [17] found that the error in the model's predictions could reach 30% for air velocity and turbulence kinetic energy in complex airflows such as forced or mixed convection.

The above challenges could be overcome through direct measurement of the whole airflow field, followed by the use of an appropriate model to predict the contaminant transport. For airflow measurements, a possible approach is particle image velocimetry (PIV), which is widely used for 2-D airflow measurements, [18], [19], [20]. A recently proposed volumetric PIV technique is the tomographic PIV system, which employs four or more cameras to measure the 3-D air velocity distribution [21]. Although 3-D airflow field measurements for a whole space are still challenging, the rapid development of advanced sensing technologies may facilitate such measurements in the near future. Therefore, it is worthwhile to explore the feasibility of predicting contaminant transport from the measured airflow field in an enclosed environment.

Furthermore, in light of the challenges in airflow field measurements, an appropriate contaminant transport model that can accommodate relatively low-resolution airflow inputs should be identified. Currently, the Eulerian and Lagrangian models are the most popular for prediction of contaminant transport. The Eulerian model solves the contaminant transport equation, while the Lagrangian model tracks each particle by solving its momentum equation [22]. Normally, these two models require the detailed airflow field as input to calculate the contaminant transport [23]. It would be challenging to use the Eulerian and Lagrangian models with relatively low-resolution or even zonal airflow input. Recently, the Markov chain model was proposed for the prediction of transient contaminant transport [24]. This model is based on the transition probabilities between zones instead of solving the contaminant transport equation. The transition probabilities are determined by the rate of airflow from the current zone to a neighboring zone. Hence, theoretically, the Markov chain model can accommodate relatively low-resolution or zonal airflow inputs [25]. Furthermore, the Markov chain model does not require iterations in each time step, and is thus more computationally efficient than the Eulerian or Lagrangian model. Therefore, this study hypothesizes that it is feasible to predict contaminant transport using the Markov chain model based on the measured airflow field in an enclosed environment.

This study first developed a stand-alone solver for the Markov chain model in MATLAB 2020a [26] that can use airflow field data as input and calculate the transient contaminant transport. An advantage of the solver is that it does not rely on any commercial software, which would facilitate future practical applications. This study applied the stand-alone Markov chain solver to three cases in which the input of the airflow field was obtained by virtual measurements based on CFD simulation. The resolution for the sampling of the virtually measured air velocities was based on the available experimental technique. The feasibility of using the Markov chain model to predict the contaminant transport from the measured airflow field was then explored by means of a case study.

2. Methods

2.1 Markov chain model

This study used the first-order homogenous Markov chain technique, in which the future state is determined by the current state and the probability that the state will change [27]. The whole airflow field is divided into $n-1$ zones, and the n^{th} zone is defined as the space where the contaminants exhaust. The contaminant quantity (mass or number) at a certain state (denoted N_k) is stored in the following vector:

$$N_k = \left(N_{k,1}\ \ N_{k,2} \ldots\ \ N_{k,n}\right) \tag{1}$$

where $N_{k,i}$ is the quantity of contaminant in zone i at state k. Note that it is assumed that in one time step, the contaminant in a certain zone can only enter the neighboring zones. Therefore, after one time step, for state $k+1$, the contaminant number in zone i can be calculated by:

$$N_{k+1,i} = N_{k,i} \cdot p_{i,i} + \sum_{nb} N_{k,nb} \cdot p_{nb,i} \tag{2}$$

where the subscript nb represents the neighboring zones to zone i. Here $p_{i,i}$ and $p_{nb,i}$ are the transition probabilities. In this work, $p_{i,i}$ is the probability that the contaminant stays in the current zone, and $p_{i,j}$ represents the transport probability that the contaminant will move from zone i to zone j. At state k, the contaminant concentration in zone i ($C_{k,i}$) can be computed by:

$$C_{k,i} = \frac{N_{k,i}}{V_i} \tag{3}$$

where V_i is the volume of zone i. The $p_{i,i}$ can be computed in accordance with the mass balance equation [28]:

$$p_{i,i} = \exp\left(-\sum_{nb} \frac{Q_{i,nb}}{V_i} \Delta t\right) \tag{4}$$

where $Q_{i,nb}$ represents the rate of airflow from zone i to the neighboring zone. Assuming that zone j is one of the neighboring zones to zone i, the $p_{i,j}$ can then be calculated by [28]:

$$p_{i,j} = \frac{Q_{i,j}}{\sum_{nb} Q_{i,nb}} \left(1 - p_{i,i}\right) \tag{5}$$

Note that within a time step (Δt), the maximum distance (s_{max}) by which the contaminant can move is the distance between the center of zone i and the furthest boundary of zone j. Assuming that the air velocity (v) from zone i to zone j is $v_{i,j}$, the maximum time step (Δt_{max}) can then be estimated by:

$$\Delta t_{max} = \frac{s_{max}}{v_{i,j}} \tag{6}$$

The time step used in this study was smaller than the Δt_{max}, in order to comply with the requirements of the first-order homogenous Markov chain model.

A mathematical solver was constructed in MATLAB 2020a [26] to execute the Markov chain model. Note that the solver developed in this study is stand-alone and does not rely on any commercial software, thus facilitating future practical applications. The input was the measured airflow field data, and the output was the transient contaminant concentration distributions, since the Markov chain model is based on the airflow and contaminant transport between zones. The rate of airflow from zone i to the neighboring zone j, $Q_{i,j}$, consists of the mean airflow rate ($Q_{mean,i,j}$) and the turbulent fluctuating airflow rate ($Q_{fluctuating,i,j}$):

$$Q_{i,j} = Q_{mean,i,j} + Q_{fluctuating,i,j} \tag{7}$$

Fig. 1 depicts the relationship between the airflow measurements and the $Q_{mean,i,j}$ and $Q_{fluctuating,i,j}$ in the Markov chain model. The three-dimensional air velocity components (u, v, w) and the turbulence kinetic energy (k) are measured at the center of each zone. The mean airflow rate from the current zone i to the neighboring zone j, $Q_{mean,i,j}$, is calculated by:

$$Q_{mean,i,j} = \frac{v_i + v_j}{2} \cdot A_{ij} \tag{8}$$

where v_i and v_j are the measured mean air velocity in the y direction in zones i and j, respectively, and A_{ij} is the area of the connecting face between zones i and j. The turbulent fluctuating airflow rate from the current zone i to the neighboring zone j, $Q_{fluctuating,i,j}$, can be calculated from the measured turbulence kinetic energy in zone i (k_i):

$$Q_{fluctuating,i,j} = \alpha_{i,j}\sqrt{2k_i/3} \cdot A_{ij} \tag{9}$$

where the coefficient $\alpha_{i,j}$ is used to characterize the influence of the distance between the two adjacent zones and the time step on the turbulent dispersion of contaminants, which can be calculated by [24]:

$$\alpha_{i,j} = 2 \cdot \left(1 - \phi\left(\frac{\Delta s_{i,j}/\Delta t}{\sqrt{2k_i/3}}\right)\right) \tag{10}$$

where $\Delta s_{i,j}$ is the distance from the centroid of zone i to that of zone j, $\phi()$ is the cumulative distribution function of a standard normal distribution:

$$\phi(x) = \frac{1}{2}\left(1 + erf\left(\frac{x}{\sqrt{2}}\right)\right) \tag{11}$$

where $erf()$ is the error function.

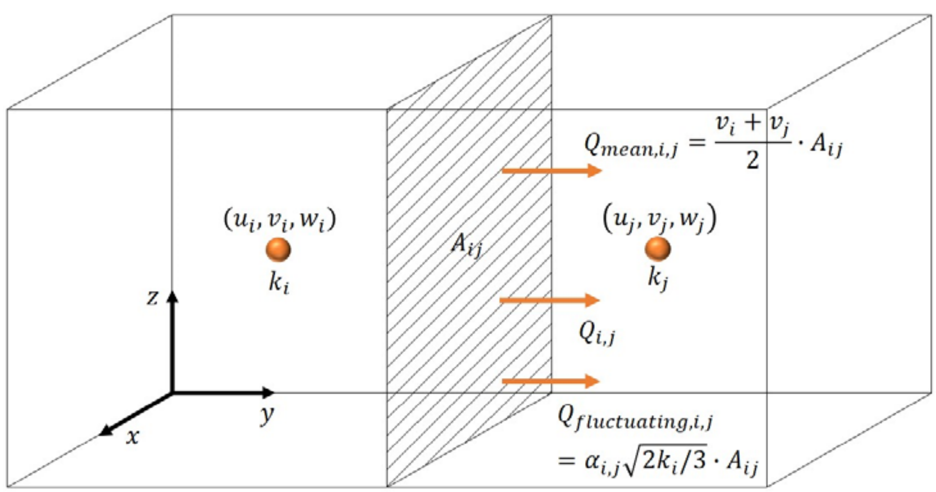

Fig. 1. Relationship between the airflow measurements and the airflow rates $Q_{mean,i,j}$ and $Q_{fluctuating,i,j}$ in the Markov chain model.

2.2 Measured airflow field

2.2.1 Possible measuring technique

Various techniques can be employed to measure the airflow field in an enclosed environment. For example, ultrasonic anemometers can be used for three-dimensional air velocity measurements. However, the size of an ultrasonic anemometer is around 0.15 m, and it may be too bulky to obtain the airflow distribution with a very high resolution. Nevertheless, since the Markov chain model can accommodate relatively low-resolution or zonal airflow inputs, the airflow field data with a resolution of 0.15 m obtained by ultrasonic anemometers may be sufficient as the input for the Markov chain model. Another potential issue is the time needed to conduct the measurements for the whole space. The traditional manual operation is not practical. However, with the rapid development of robotic technologies, automated measurements with ultrasonic anemometers, like using cable-driven robots with routing design [29] or robotic arms equipped with probes [30] will significantly reduce the time cost and enable whole-space measurements in the near future.

A number of other techniques can be potentially used for whole-space airflow measurements in a rapid and non-invasive manner. For example, particle image velocimetry can be employed to characterize the airflow in an enclosed environment. The most frequently used PIV system can only measure the two-dimensional airflow field [20], which is insufficient as the input for the Markov chain model. To obtain the three-dimensional airflow field, volumetric PIV systems such as the tomographic PIV system can be used. However, since volumetric PIV systems require four or more cameras [21], they are expensive and complicated, and therefore may not be suitable for practical applications. Light detection and ranging (LIDAR) is another potential technique for whole-space airflow measurements in the future. LIDAR is a remote sensing technology that has been widely used in atmospheric physics to measure parameters such as temperature, pressure, humidity, and wind, and to detect substances such as trace gases, clouds, and aerosols [31]. In the future, if volumetric PIV systems have advanced to affordable and portable instruments or if the LIDAR technique is further developed for indoor applications, the proposed method for predicting contaminant transport from the measured airflow field would become easier and more practical.

2.2.2 Virtually measured airflow field

Currently, the feasibility of predicting contaminant transport from the measured airflow fields with relatively low resolution is unclear. To preliminarily explore this hypothesis, this study conducted computer experiments based on CFD simulations by commercial software code ANSYS Fluent [32]. Namely, the high-resolution airflow field calculated by CFD with fine grids was treated as the “true” airflow. To mimic whole-space airflow measurements using ultrasonic anemometers, the airflow data, including the three-dimensional air velocity components and turbulence kinetic energy, were sampled virtually on the basis of a 0.15-m resolution. The virtually measured airflow data were then used as input for the Markov chain model to predict contaminant transport in the space using the MATLAB stand-alone solver developed in this study. The RNG k-ε model was used to calculate the airflow and turbulence, as recommended for enclosed environments [16]. The equations for the model can be found in the ANSYS Fluent manual [33].

2.3 Grid strategy for Markov chain calculation

The grid used for Markov chain calculation in this study was hexahedral, and it was determined from both the airflow sampling points and the geometric properties of the boundary zones. The grid was constructed with the air sampling points taken as the centroid of each cell. The airflow field inside each cell was assumed to be uniform, and the airflow properties on a cell face were determined by its two connecting cells. However, the size of the boundary zones might be smaller than that of the constructed corresponding cells. For accurate set-up of the boundary conditions, the cells required further refinement. An example of the grid refinement strategy is provided in Fig. 2. Here, Fig. 2(a) shows a cell constructed according to the airflow sampling point with a sampling resolution of 0.15 m; thus, the cell size is 0.15 m × 0.15 m × 0.15 m. The size of the contaminant source is smaller than the cell size. Fig. 2(b) shows the refined cell based on the size of the contaminant source, and the division of the original cell into 18 cells. The airflow data in the 18 cells were set the same as that of the original cell. With this effort, the grid can truly reflect the sizes of the boundaries and improve the performance of the model.

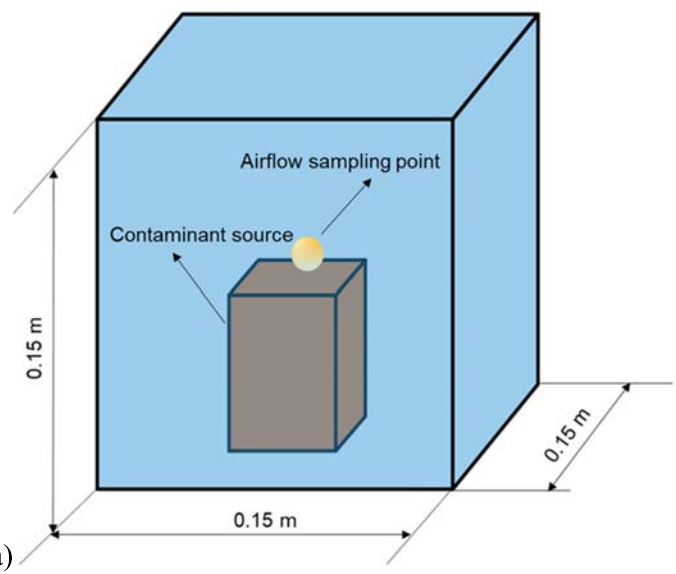

(a)

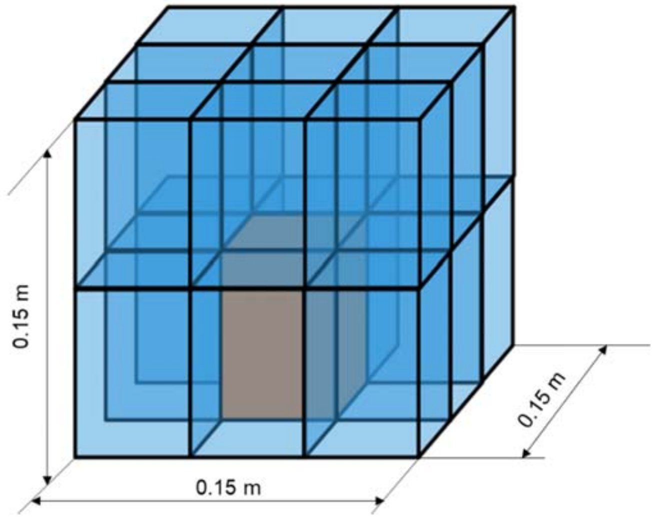

(b)

Fig. 2. Example of grid refinement for Markov chain calculation: (a) a cell constructed according to the airflow sampling point with a sampling resolution of 0.15 m, and (b) the refined cell based on the size of the contaminant source.

3. Benchmark for contaminant transport

Ideally, the benchmark for evaluating the stand-alone Markov chain solver should be obtained by means of high-quality airflow and contaminant transport measurements. For preliminary analysis, this study conducted computer experiments as a proof of concept. Calculated contaminant transport results based on CFD simulations were used as the benchmark. The CFD simulation in this study employed the Fluent-based Markov chain solver developed by Chen et al. [24] for calculating contaminant transport. To ensure that the benchmark results were reasonably accurate, the CFD program was validated by experimental data from Zhang et al. [34]. Fig. 3 shows the chamber used by Zhang et al. [34], of which the dimensions were 4 m (L) × 2.1 m (W) × 2.4 m (H). A supply air inlet was installed on one of the side walls at a distance of 0.3 m from the ceiling. The outlet was installed on the opposite side wall, at a height of 0.3 m above the floor. Both the inlet and outlet had dimensions of 0.3 m × 0.3 m. The average velocity of the supply air was 0.84 m/s; the supply air angle was 10^{o} downward; and the turbulence intensity was 20%. Particles with diameter of 1 μm were injected into the chamber through the inlet. The transient particle concentrations were measured by Zhang et al. [34] at two positions as shown in Fig. 3, and were used for model validation.

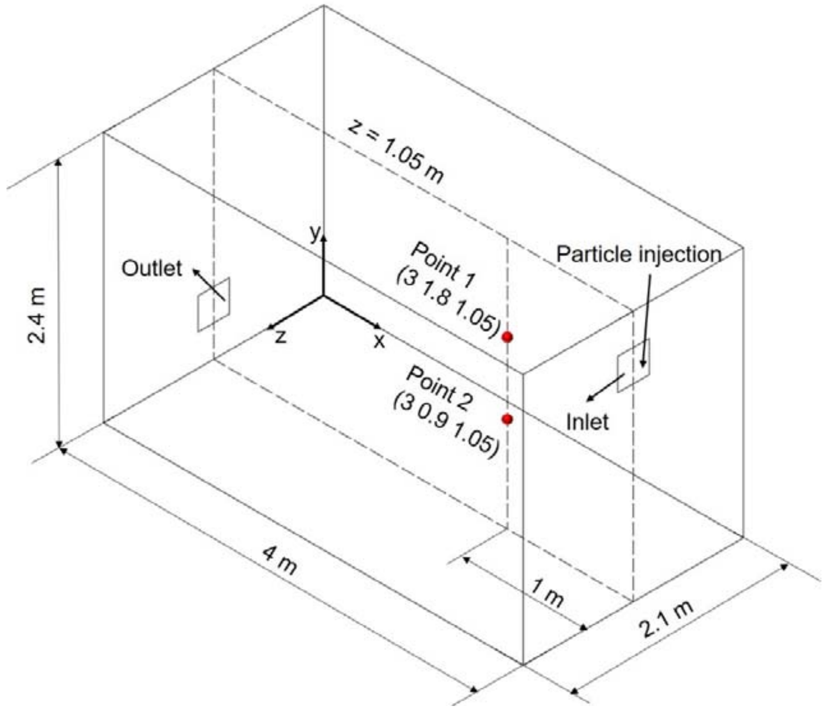

Fig. 3. Schematic of the chamber for the particle transport experiment by Zhang et al. [34].

The airflow field was obtained with the use of the RNG k-ε model. A grid independence test was conducted, and the grid resolution of 32,480 was found to be sufficiently fine. The time step size for calculating the transient transport was set at 0.01 s. Fig. 4 compares the transient particle concentrations obtained by the CFD simulations and the experimental data. In general, the calculated results from the CFD simulations captured the peaks of the contaminant transport. Although there were some discrepancies between the calculated results and the experimental data, the calculated results from the CFD simulations in this study were close to those calculated by Zhang et al. [34]. Note that in Fig. 4 (b), the results simulated by Zhang et al. [34] was smoother than the calculated results in this study. The reason is the time step was set at 0.01 s in this study, while that used by Zhang et al. [34] was 1 s. Therefore, the CFD models in this study predicted the trend of transient contaminant transport reasonably well, and could be used as the benchmark for comparison.

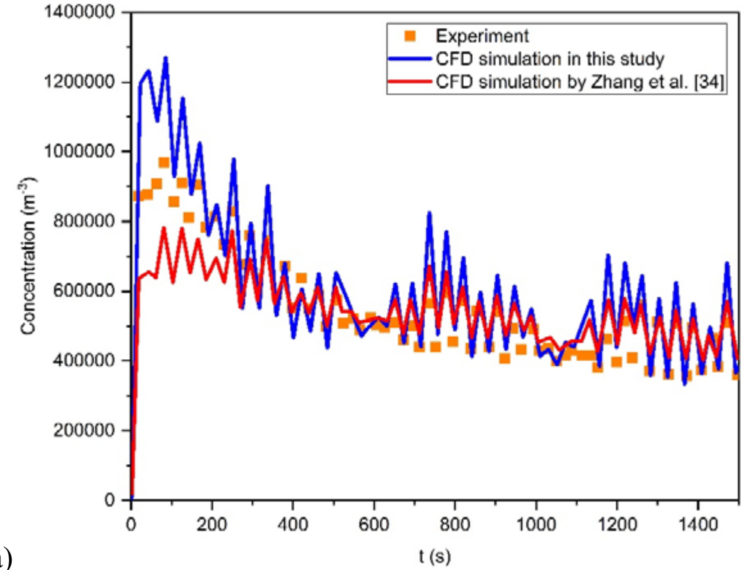

(a)

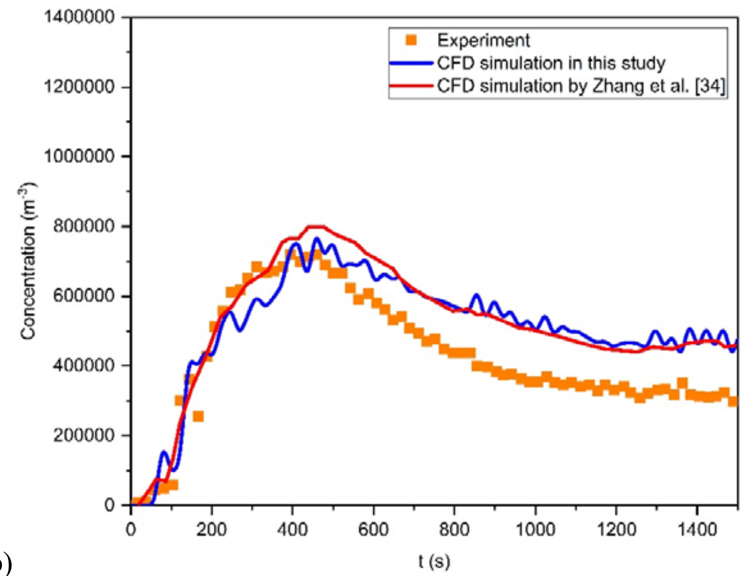

(b)

Fig. 4. Comparison of transient particle concentrations calculated by the CFD-Markov chain model based on commercial CFD software and the experimental data at the two measuring locations: (a) height = 1.8 m and (b) height = 0.9 m.

4. Case study

In this study, three cases were used to explore the feasibility of predicting contaminant transport from the measured airflow field. The three cases focused on the transient contaminant transport in ventilated chambers under isothermal conditions, with one heat source, and with two occupants seated face to face, respectively. For all the cases, the benchmark results were the transient contaminant transport calculated by the validated Fluent-based Markov chain solver with a high-resolution grid. Based on the "true" airflow field calculated by CFD, the three-dimensional air velocity components and turbulence kinetic energy with a 0.15-m resolution (the highest resolution that can be achieved when using ultrasonic anemometers) were virtually sampled. With the virtually measured airflow data as input, the MATLAB stand-alone Markov chain solver developed in this study was used to calculate the contaminant transport. The results were normalized by the maximum concentrations at the initial state:

$$C_k^* = \frac{C_k}{C_{0(max)}} \quad (12)$$

where C_k and C_k^* respectively represent the calculated and normalized concentrations at state k, and $C_{0(max)}$ is the maximum concentration at the initial state. The normalized results were then compared with the benchmark to assess the feasibility of predicting contaminant transport from the measured airflow field.

4.1 Case 1: Contaminant transport in an isothermal ventilated chamber

The configuration of the chamber in Case 1 is shown in Fig. 3. The thermo-fluid boundary conditions were the same as those in the validation case. The benchmark CFD calculation was based on a total grid number of 32,480. Fig. 5 shows the distribution of the airflow sampling points based on a 0.15 m resolution. Note that due to geometric constraints, some of the sampling points close to the walls may not be exactly at the interval of 0.15 m. In total, the airflow measurements were conducted at 5,265 points. The Markov chain grid was constructed on the basis of the airflow sampling points and the geometric characteristics of boundary zones, as described in Section 2.2.3. The final Markov chain grid number was 7,695. The contaminants were injected into the chamber through the supply air inlet for 0.1 s. The time step size was set at 0.1 s.

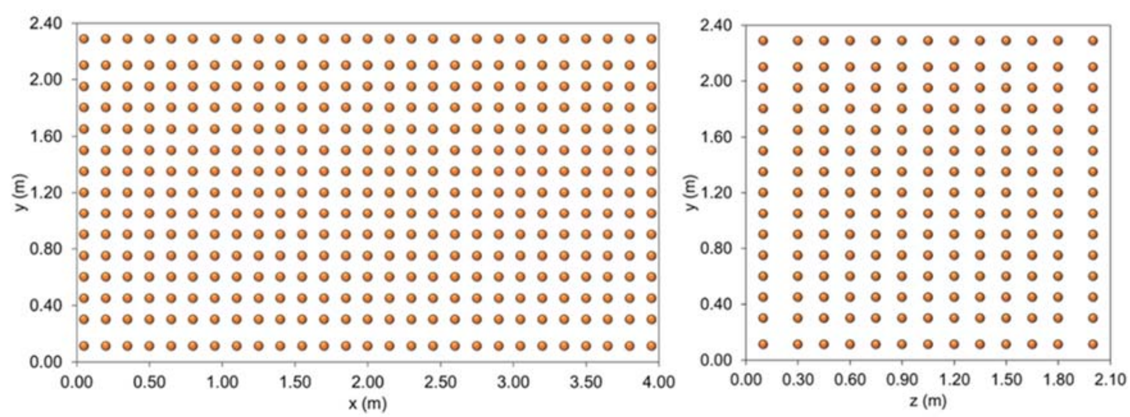

Fig. 5. Distribution of the airflow sampling points with a resolution of 0.15 m for Case 1.

Fig. 6 depicts the transient contaminant transport in the first 10 s at the cross-section of the central z-plane. The general trend of the contaminant transport calculated using the stand-alone Markov chain solver based on the measured airflow field was in good agreement with the benchmark. Furthermore, the location and time at which the maximum contaminant concentration occurred were also correctly predicted. Therefore, the computer experiment for

Case 1 partially demonstrated the feasibility of using the stand-alone Markov chain solver to predict contaminant transport from the three-dimensional air velocity components and turbulence kinetic energy in the whole chamber measured by ultrasonic anemometers.

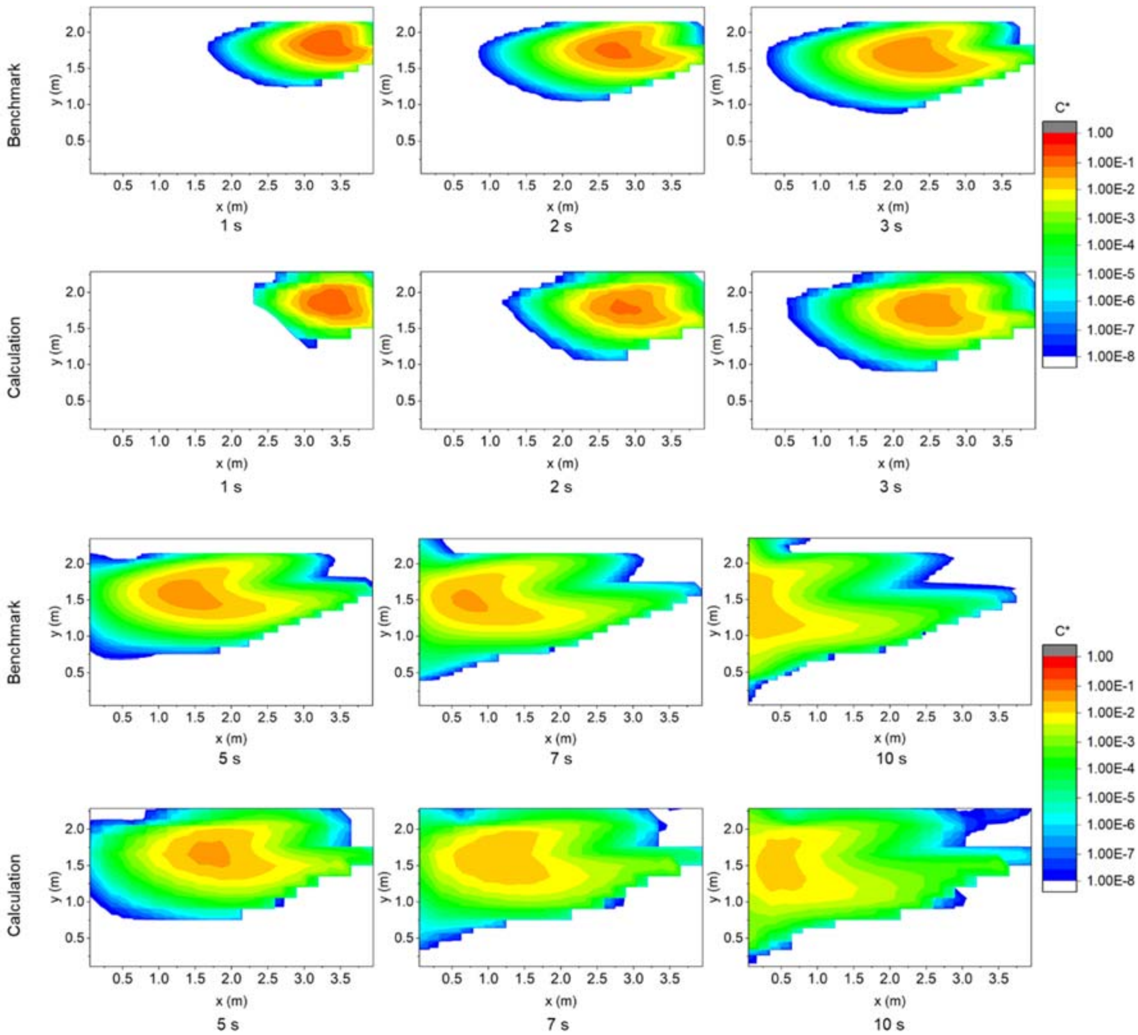

Fig. 6. Comparison of the contaminant transport between the benchmark and the results calculated from the measured airflow field at a 0.15-m resolution using the stand-alone Markov chain solver for Case 1.

4.2 Case 2: Contaminant transport in a ventilated chamber with a heat source

A schematic of the ventilated chamber for Case 2 [35] is shown in Fig. 7. The dimensions of the chamber were 2.6 m, 1.3 m and 1.8 m in length, width and height, respectively. Four 2.5-cm wide slots were installed at the edges of the floor to supply cool air at 20 °C with a velocity of 0.08 m/s and turbulence intensity of 10%. Two outlets with dimensions of 0.2 m × 0.2 m were located on the ceiling. Meanwhile, a 0.2 m (L) × 0.2 m (W) × 0.22 m (H) heat source at the center of the floor had a heat generation rate of 65 W. The contaminant source was located above the heat source, and it was set as a pulse source within the duration of 0.2 s. A grid resolution of 53,740 was used for the airflow calculation in accordance with a grid independence test. Fig. 8 shows the distribution of the airflow measuring points based on a resolution of 0.15 m. There was a total of 1,155 points for the airflow measurements. The Markov chain grid was then constructed on the basis of the airflow sampling points and the sizes of boundary zones, and the total grid number was 1,683. The time step size for contaminant transport calculation was set at 0.2 s for Case 2.

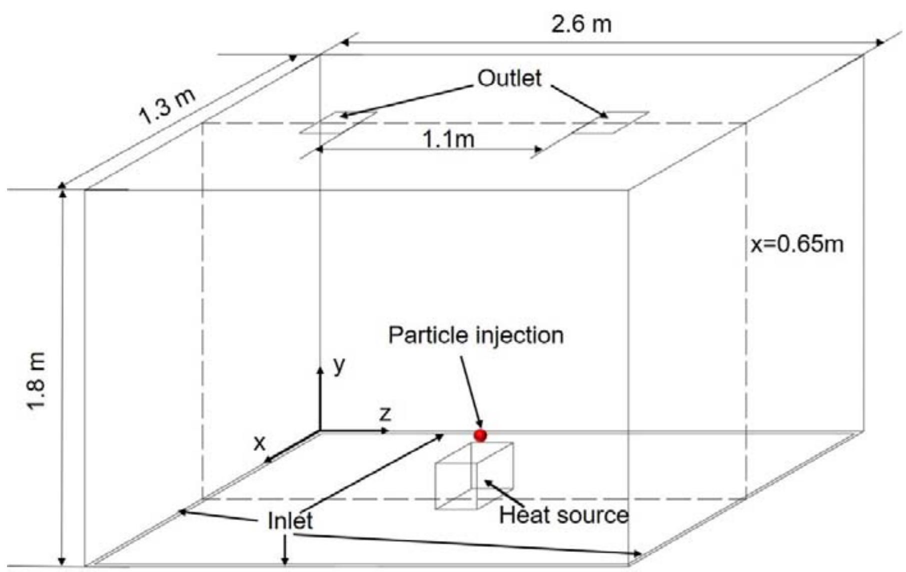

Fig. 7. Schematic of the chamber for Case 2 studied by Bolster and Linden [35].

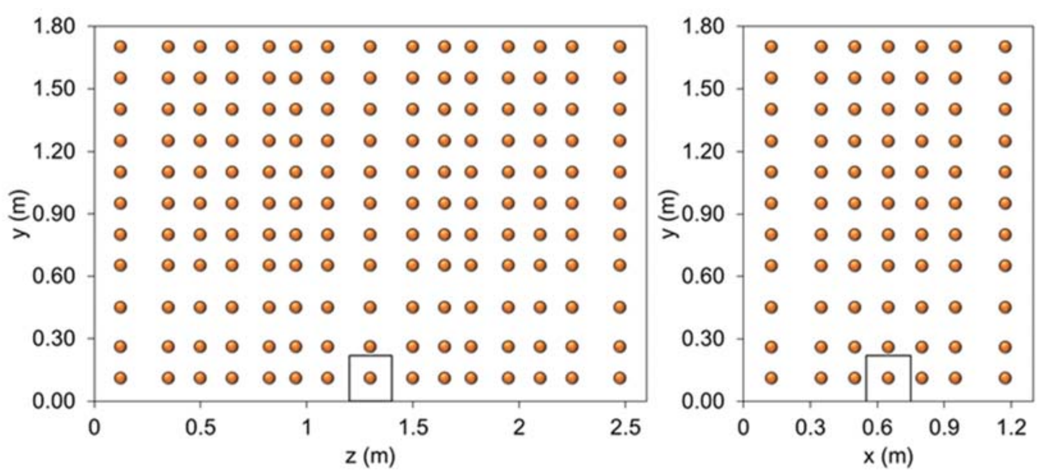

Fig. 8. Distribution of the airflow sampling points with a resolution of 0.15 m for Case 2.

Fig. 9 compares the contaminant transport in the first 5 s at the cross section of the central x-plane from the benchmark and the stand-alone Markov chain solver. The comparison shows that the stand-alone Markov chain solver based on the measured airflow field provided a reasonably good prediction of the upward transport of the contaminants, which was mainly driven by the thermal plume generated by the heat source. However, in the first 3 s, the maximum contaminant concentration calculated from the stand-alone Markov chain solver was lower than that of the benchmark. From the benchmark, the contaminant concentration gradients in the z direction were obvious in the first 3 s. However, the gradients were not reflected due to the relatively large airflow sampling cell with a 0.15 m resolution. Therefore, if the objective is to obtain the general trend of contaminant transport, the stand-alone Markov chain solver based on the measured airflow field can be used. However, if the detailed concentration gradients need to be captured, the proposed method may not be appropriate.

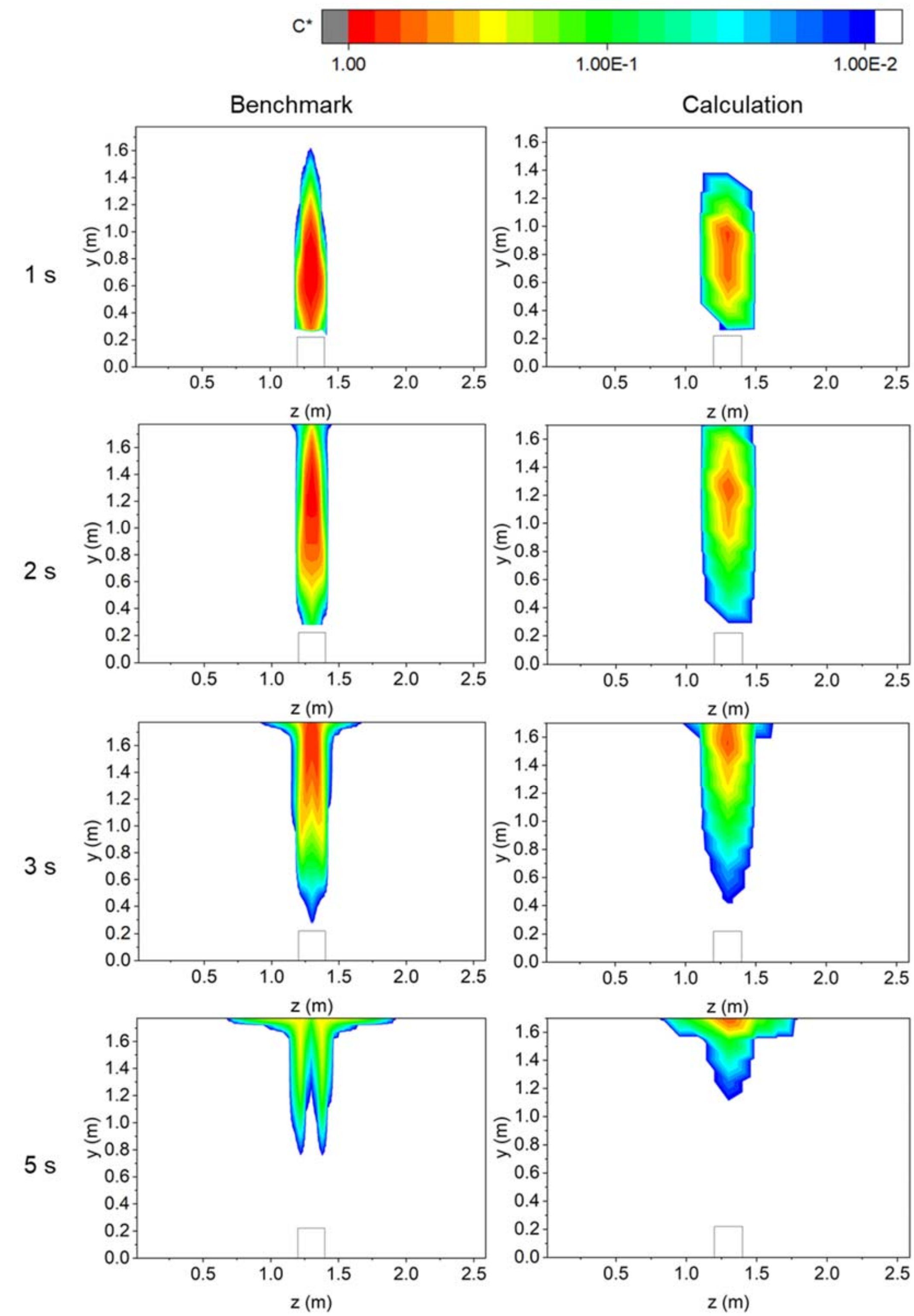

Fig. 9. Comparison of the contaminant transport between the benchmark and the results calculated from the measured airflow field at a 0.15-m resolution using the stand-alone Markov chain solver for Case 2.

4.3 Case 3: Person-to-person contaminant transport in a ventilated chamber

The configuration of the ventilated chamber with two occupants seated face to face [36] is shown in Fig. 10. The dimensions of the chamber were 3 m (L) × 3 m (W) × 2.3 m (H). The distance between the occupants was approximately 1 m. The contaminants were released in the breathing zone of one occupant, which was assumed to be a single pulse source within the duration of 0.2 s. It was assumed that the mouth and nose of the occupant were covered with a tissue, and the initial momentum of the exhaled contaminant was neglected [36]. The supply air inlet was installed on the side wall near the ceiling, and the outlet was installed on the same wall but near the floor. The air exchange rate was 3 ACH, and the supply air temperature was 21 °C. The surface temperature of the human bodies was 32 °C. The airflow was calculated by CFD with a grid resolution of 1,415,560, which passed the grid independence test. The distribution of the airflow measuring points based on a resolution of 0.15 m is shown in Fig. 11. Note that at the locations near boundaries such as walls and occupants, the airflow sampling cells were larger due to the limitation of geometric structure. In total, there were 3,952 airflow sampling points. The Markov chain grid was then constructed with a grid number of 5,712 based on the airflow sampling points and sizes of boundary zones. The calculated contaminant concentrations were normalized by the maximum concentration at the source. The time step size was set at 0.2 s for Case 3.

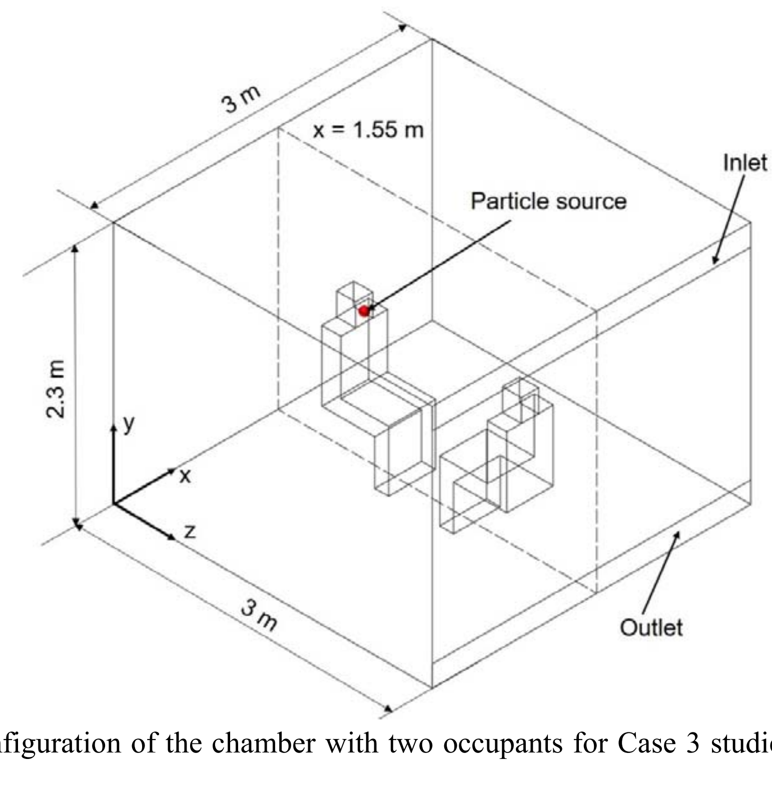

Fig. 10. Configuration of the chamber with two occupants for Case 3 studied by Chen et al. [36].

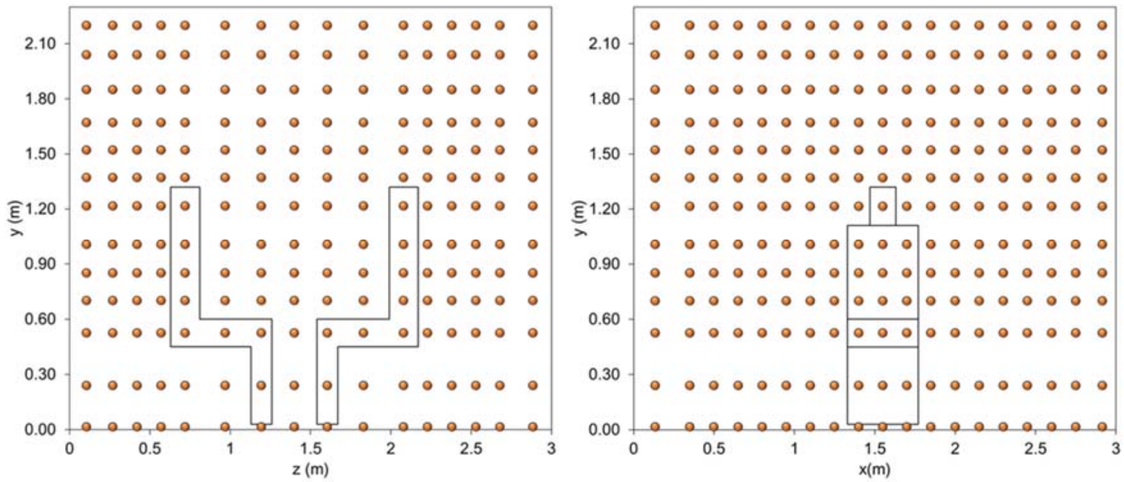

Fig. 11. Distribution of the airflow sampling points with a 0.15 m resolution for Case 3.

The results for transient contaminant transport in the first 10 s at the cross-section of plane x = 1.55 m are shown in Fig. 12. The stand-alone Markov chain solver based on the measured airflow field predicted the general trend of contaminant transport reasonably well when compared with the benchmark. However, the solver calculated more disperse concentration patterns than did the benchmark. This was because the use of coarse airflow sampling grids led to failure in predicting the high-gradient concentration regions. Therefore, as in Case 2, if the aim is to obtain the general contaminant transport trend, the stand-alone Markov chain solver based on measured airflow field can be used effectively. However, if capturing the detailed concentration gradients is crucial, the proposed method will not be feasible.

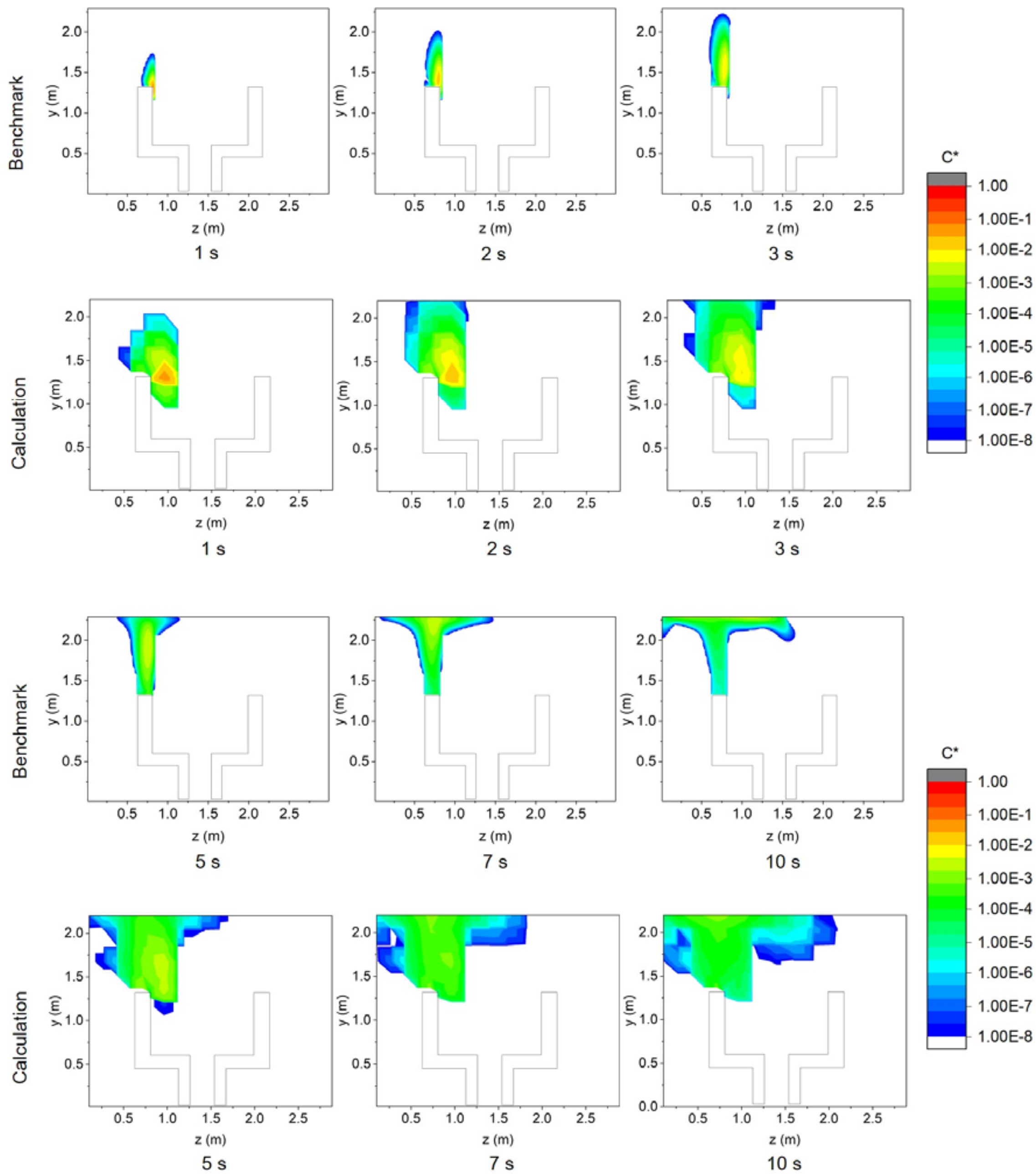

Fig. 12. Comparison of the contaminant transport between the benchmark and the results calculated from the measured airflow field at a 0.15-m resolution using the stand-alone Markov chain solver for Case 3.

5. Discussion

In practical applications, such as hospital wards [6], aircraft cabins [37], and restaurants [38], where many cross-infections have occurred, it may be challenging to measure the complex thermo-fluid boundary conditions. Furthermore, the existing turbulence model may be yield accurate airflow distribution in those complex environments. Consequently, the existing approach of using commercial CFD software to predict contaminant transport may not be effective. Therefore, this study aimed to preliminarily explore the feasibility of predicting the contaminant transport using a stand-alone Markov chain solver based on the measured airflow field in an enclosed environment. Note that the source location and strength need to be provided in the calculations. According to the computer experiments presented in this study, if the airflow is simple, such as in the isothermal Case 1, the stand-alone Markov chain solver based on the measured airflow field can predict the trend of contaminant transport and peak concentrations reasonably well. However, if the airflow is complex, such as in the non-isothermal Cases 2 and 3, the stand-alone Markov chain solver based on the measured airflow field can reasonably predict only the general trend of contaminant transport. Besides, the developed Markov chain solver in this study aims for the contaminant transport in a steady airflow field. For transient airflow fields, for example, considering natural ventilation, moving occupants, and door and window behaviors, the solver cannot be directly implemented. It should be noted that the capability of the proposed method depends strongly on the resolution of the airflow measurements. This study used a resolution of 0.15 m that was based on the size of the ultrasonic anemometer. In the future, if non-invasive airflow measuring techniques such as volumetric PIV [21] and LIDAR [31] systems have advanced to an affordable and portable level, the applicability of the stand-alone Markov chain solver based on the measured airflow field will be extended. Furthermore, it would be worthwhile to conduct field measurements of whole-space airflow to further demonstrate the feasibility of the proposed approach. Currently, the challenges are the time and effort needed for manual operation of the measurements if ultrasonic anemometers are used. A cable robot-based automated measuring system is under development, which would facilitate on-site measurements in the future.

6. Conclusions

This study explored the feasibility of using a Markov chain model to predict contaminant transport from the measured airflow field in an indoor environment. A stand-alone Markov chain solver was developed so that the calculations need not rely on commercial software. The required airflow information, including the three-dimensional velocity components and turbulence kinetic energy, was obtained on the basis of the resolution of ultrasonic anemometers (0.15 m), via virtual airflow measurements simulated by CFD. Three cases were used to investigate the feasibility of the proposed method, and the calculation results were compared with the benchmark calculated by the commercial CFD software. The following conclusions can be drawn:

(1) When the airflow is simple, such as in the isothermal Case 1, the stand-alone Markov chain solver based on the measured airflow field can predict the trend of contaminant transport and peak concentrations reasonably well.

(2) When the airflow is complex, such as in the non-isothermal Cases 2 and 3, the stand-alone Markov chain solver based on the measured airflow field can reasonably predict only the general trend of contaminant transport.

Acknowledgement

This work was supported by the Early Career Scheme of Research Grants Council of Hong Kong SAR, China (Grant No. 25210419).

References

[1] P.J. Edelson, Patterns of measles transmission among airplane travelers, Travel Med. Infect. Dis. 10 (2012) 230-235, https://doi.org/10.1016/j.tmaid.2012.10.003.

[2] Z. Shen, F. Ning, W. Zhou, X. He, C. Lin, D.P. Chin, et al., Superspreading SARS events, Beijing, 2003, Emerg. Infect. Dis. 10 (2004) 256-260, https://doi.org/10.3201/eid1002.030732.

[3] G. Chowell, S.M. Bertozzi, M.A. Colchero, H. Lopez-Gatell, C. Alpuche-Aranda, M. Hernandez, et al., Severe respiratory disease concurrent with the circulation of H1N1 influenza, N. Engl. J. Med. 361 (2009) 674-679, https://doi.org/10.1056/NEJMoa0904023.

[4] N. Zhu, D. Zhang, W. Wang, X. Li, B. Yang, J. Song, et al., A novel coronavirus from patients with pneumonia in China, 2019, N. Engl. J. Med. 382 (2020) 727-733, https://doi.org/10.1056/NEJMoa2001017.

[5] Y. Li, G.M. Leung, J.W. Tang, X. Yang, C.Y. Chao, J.Z. Lin, et al., Role of ventilation in airborne transmission of infectious agents in the built environment - a multidisciplinary systematic review, Indoor Air 17 (2007) 2-18, https://doi.org/10.1111/j.1600-0668.2006.00445.x.

[6] Y. Liu, Z. Ning, Y. Chen, M. Guo, Y. Liu, N.K. Gali, et al., Aerodynamic analysis of SARS-CoV-2 in two Wuhan hospitals, Nature 582 (2020) 557-560, https://doi.org/10.1038/s41586-020-2271-3.

[7] Q. Chen, Can we migrate COVID-19 spreading risk?, Front. Environ. Sci. Eng. 15 (2021) 35, https://doi.org/10.1007/s11783-020-1328-8.

[8] J. Wei, Y. Li, Airborne spread of infectious agents in the indoor environment, Am. J. Infect. Control. 44 (2016) S102-108, https://doi.org/10.1016/j.ajic.2016.06.003.

[9] B. Zhao, C. Yang, C. Chen, C. Feng, X. Yang, L. Sun, et al., How many airborne particles emitted from a nurse will reach the breathing zone/body surface of the patient in ISO Class-5 single-bed hospital protective environments?—A numerical analysis, Aerosol Sci. Technol. 43 (2009) 990-1005, https://doi.org/10.1080/02786820903107925.

[10] N.E. Klepeis, W.C. Neilson, W.R. Ott, J.P. Robinson, A.M. Tsang, P. Switzer, et al., The National Human Activity Pattern Survey (NHAPS): a resource for assessing exposure to environmental pollutants, J. Exposure Sci. Environ. Epidemiol. 11 (2001) 231-252, https://doi.org/10.1038/sj.jea.7500165.

[11] Z. Zhang, Q. Chen, Experimental measurements and numerical simulations of particle transport and distribution in ventilated rooms, Atmos. Environ. 40 (2006) 3396-3408, https://doi.org/10.1016/j.atmosenv.2006.01.014.

[12] Y. Pan, C.-H. Lin, D. Wei, C. Chen, Experimental measurements and large eddy simulation of particle deposition distribution around a multi-slot diffuser, Build. Environ. 150 (2019) 156-163, https://doi.org/10.1016/j.buildenv.2019.01.011.

[13] Z. Zhang, X. Chen, S. Mazumdar, T. Zhang, Q. Chen, Experimental and numerical investigation of airflow and contaminant transport in an airliner cabin mockup, Build. Environ. 44 (2009) 85-94, https://doi.org/10.1016/j.buildenv.2008.01.012.

[14] C. Chen, W. Liu, F. Li, C.H. Lin, J. Liu, J. Pei, et al., A hybrid model for investigating transient particle transport in enclosed environments, Build. Environ. 62 (2013) 45-54, https://doi.org/10.1016/j.buildenv.2012.12.020.

[15] V. Blanes-Vidal, E. Guijarro, S. Balasch, A.G. Torres, Application of computational fluid dynamics to the prediction of airflow in a mechanically ventilated commercial poultry building, Biosyst. Eng. 100 (2008) 105-116, https://doi.org/10.1016/j.biosystemseng.2008.02.004.

[16] Z. Zhang, W. Zhang, Z. Zhai, Q. Chen, Evaluation of various turbulence models in predicting airflow and turbulence in enclosed environments by CFD: Part 2—Comparison with experimental data from literature, HVAC&R Res. 13 (2007) 871-886, http://dx.doi.org/10.1080/10789669.2007.10391460.

[17] M. Wang, Q. Chen, Assessment of Various Turbulence Models for Transitional Flows in an Enclosed Environment (RP-1271), HVAC&R Res. 15 (2009) 1099-1119, http://dx.doi.org/10.1080/10789669.2009.10390881.

[18] R. You, J. Chen, Z. Shi, W. Liu, C.-H. Lin, D. Wei, et al., Experimental and numerical study of airflow distribution in an aircraft cabin mock-up with a gasper on, J. Build. Perform. Simul. 9 (2016) 555-566, https://doi.org/10.1080/19401493.2015.1126762.

[19] R. You, Y. Zhang, X. Zhao, C.H. Lin, D. Wei, J. Liu, et al., An innovative personalized displacement ventilation system for airliner cabins, Build. Environ. 137 (2018) 41-50, https://doi.org/10.1016/j.buildenv.2018.03.057.

[20] A. Li, E. Qin, B. Xin, G. Wanga, J. Wang, Experimental analysis on the air distribution of powerhouse of Hohhot hydropower station with 2D-PIV, Energy Convers. Manage. 51 (2010) 33-41, https://doi.org/10.1016/j.enconman.2009.08.022.

[21] X. Cao, J. Liu, N. Jiang, Q. Chen, Particle image velocimetry measurement of indoor airflow field: A review of the technologies and applications, Energy Build. 69 (2014) 367-380, https://doi.org/10.1016/j.enbuild.2013.11.012.

[22] Z. Zhang, Q. Chen, Comparison of the Eulerian and Lagrangian methods for predicting

particle transport in enclosed spaces, Atmos. Environ. 41 (2007) 5236-5248, http://doi.org/10.1016/j.atmosenv.2006.05.086.

[23] C. Chen, W. Liu, C.-H. Lin, Q. Chen, Comparing the Markov chain model with the Eulerian and Lagrangian models for indoor transient particle transport simulations, Aerosol Sci. Technol. 49 (2015) 857-871, https://doi.org/10.1080/02786826.2015.1079587.

[24] C. Chen, W. Liu, C.H. Lin, Q. Chen, A Markov chain model for predicting transient particle transport in enclosed environments, Build. Environ. 90 (2015) 30-36, https://doi.org/10.1016/j.buildenv.2015.03.024.

[25] C. Chen, C.H. Lin, Z. Long, Q. Chen, Predicting transient particle transport in enclosed environments with the combined computational fluid dynamics and Markov chain method, Indoor Air 24 (2014) 81-92, https://doi.org/10.1111/ina.12056.

[26] MATLAB 2020a, MathWorks, Massachusetts, USA, 2019, https://www.mathworks.com.

[27] S.M. Ross, Stochastic Processes, 2nd ed., John Wiley & Sons, Inc, New York, 1996, https://www.academia.edu/download/56739884/stochastic-processes-ross_2.pdf.

[28] M. Nicas, Markov modeling of contaminant concentrations in indoor air, Am. Ind. Hyg. Assoc. J. 61 (2000) 484-491, https://doi.org/10.1080/15298660008984559.

[29] Y. Wang, C. Song, T. Zheng, D. Lau, K. Yang, G. Yang, Cable routing design and performance evaluation for multi-link cable-driven robots with minimal number of actuating cables, IEEE Access 7 (2019) 135790-135800, https://doi.org/10.1109/access.2019.2924982.

[30] Z. Jiang, L. Zhang, T. Qiu, Automatic high-precision measurement technology of special-shaped surface parts based on robot arms, J. Phys. Conf. Ser. 1693 (2020) 012214, https://doi.org/10.1088/1742-6596/1693/1/012214.

[31] C. Weitkamp, Lidar: Range-resolved optical remote sensing of the atmosphere, Springer Science & Business Media Inc, New York, 2006, https://books.google.com.hk/books?id=QWzrBwAAQBAJ&lpg=PR5&ots=1Pg5S1jzcZ&lr&pg=PR4#v=onepage&q&f=false.

[32] Ansys. Fluent 18.0 documentation, Fluent Inc., Lebanon, NH, 2017, https://www.ansys.com.

[33] D. Choudhury, Introduction to the renormalization group method and turbulence modeling, Fluent Inc, Canonsburg, 1993, https://scholar.google.com/scholar?cluster=4328034131192122287&hl=en&as_sdt=2005&sciodt=0,5.

[34] N. Zhang, Z. Zheng, S. Eckels, V.B. Nadella, X. Sun, Transient response of particle distribution in a chamber to transient particle injection, Part. Part. Syst. Charact. 26 (2009) 199-209, https://doi.org/10.1002/ppsc.200800043.

[35] D.T. Bolster, P.F. Linden, Particle transport in low-energy ventilation systems. Part 2: Transients and experiments, Indoor Air 19 (2009) 130-144, https://doi.org/10.1111/j.1600-0668.2008.00569.x.

[36] C. Chen, C.H. Lin, Z. Jiang, Q. Chen, Simplified models for exhaled airflow from a cough with the mouth covered, Indoor Air 24 (2014) 580-591, https://doi.org/10.1111/ina.12109.

[37] S.J. Olsen, H.-L. Chang, T.Y.-Y. Cheung, A.F.-Y. Tang, T.L. Fisk, S.P.-L. Ooi, et al., Transmission of the Severe Acute Respiratory Syndrome on Aircraft, N. Engl. J. Med. 349 (2003) 2417-2422, https://doi.org/10.1056/NEJMoa031349.

[38] Y. Li, H. Qian, J. Hang, X. Chen, P. Cheng, H. Ling, et al., Probable airborne transmission of SARS-CoV-2 in a poorly ventilated restaurant, Build. Environ. 196 (2021) 107788, https://doi.org/10.1016/j.buildenv.2021.107788.